

Real Scale Ray Tracing Simulation of Space Earthshine Measurement with Improved BRDF Model of Lunar Surface

Jinhee Yu^{a,b,c}, Dongok Ryu^{a,b}, Sung-Ho Ahn^d, Sug-Whan Kim^{a,b,c}

^aSpace Optics Laboratory, Yonsei University, 134 Sinchon-dong, Seodaemun-gu, Seoul 120-749, Republic of Korea

^bInstitute of Space Science and Technology, Yonsei University, 134 Sinchon-dong, Seodaemun-gu, Seoul 120-749, Republic of Korea

^cYonsei University Observatory, Yonsei University, 134 Sinchon-dong, Seodaemun-gu, Seoul 120-749, Republic of Korea

^dCenter for Galaxy Evolution Research, Yonsei University, 134 Sinchon-dong, Seodaemun-gu, Seoul 120-749, Republic of Korea

ABSTRACT

The discrepancy in annual changes of Earth albedo anomaly among the Had3CM prediction, ground and low Earth orbit measurements attracts great academic attention world-wide. As a part of our on-going study for better understanding of such discrepancy, we report a new earthshine measurement simulation technique. It combines the light source (the Sun), targets (the Earth and the Moon) and a hypothetical detector in a real scale Integrated Monte-Carlo Ray Tracing (IRT) computation environment. The Sun is expressed as a Lambertian scattering sphere, emitting $1.626 \times 10^{26} W$ over $400nm-750nm$ in wavelength range. Whilst we are in the process of developing a complex Earth model consisting of land, sea and atmosphere with appropriate BRDF models, a simplified Lambertian Earth surface with 0.3 in uniform albedo was used in this study. For the moon surface, Hapke's BRDF model is used with double Henry-Green phase function. These elements were then imported into the IRT computation of radiative transfer between their surfaces. First, the irradiance levels of earthshine and moonshine lights were computed and then confirmed that they agree well with the measurement data from Big Bear Solar Observatory. They were subsequently used in determination of the Earth bond albedo of about 0.3 that is almost identical to the input Earth albedo of 0.3. These computations prove that, for the first time, the real scale IRT model was successfully deployed for the Earthshine measurement simulation and, therefore, it can be applicable for other ground and space based measurement simulation of reflected lights from the Earth and the Moon.

Keywords: Integrated Ray Tracing (IRT), lunar optical model, BRDF, real scale 3D model, moonshine, earthshine, Earth albedo

1. INTRODUCTION

Long term trend of the Earth surface temperature variation is one of the central issues in climate study and hence attracts great attentions from world-wide academic communities. Global Earth bond albedo A_{Earth} plays a critical role in determination of the Earth surface temperature T_{Earth} (K) as expressed in Eq. 1, where S is the solar constant on the Earth, σ is the Stefan-Boltzmann constant and g is the normalized greenhouse effect^[1]. Two different measurement techniques for A_{Earth} have been developed and are currently used; i) direct Earth reflectance measurement with CERES instrument from low Earth orbit^[2,3] and ii) earthshine measurement from ground observatory including Big Bear Solar Observatory (BBSO, Earthshine)^[1,4-10].

Further author information: (Send correspondence to Jinhee Yu)

Jinhee Yu; E-mail: jennybizakyu@gmail.com; Phone: 82-10-3068-7706; Fax: 82-2-392-7680

UV/Optical/IR Space Telescopes and Instruments: Innovative Technologies and Concepts V,
edited by Howard A. MacEwen, James B. Breckinridge, Proc. of SPIE Vol. 8146, 81460X · © 2011 SPIE
CCC code: 0277-786X/11/\$18 · doi: 10.1117/12.893367

Proc. of SPIE Vol. 8146 81460X-1

However, the methods produced discrepancy in the Earth albedo anomaly trend as shown in Fig. 1a^[3]. More recently, the subsequent measurements and inter-instrument recalibration efforts have reduced the magnitude of the discrepancy, but the trend is still persisting as shown in Fig. 1b^[10]. This discrepancy is further aggravated when they do not agree with the climate model prediction such as ISCCP or Had3CM^[10-12]. In order to improve our understanding this discrepancy, we suggested SALEX instrument^[13] for determination of the Earth global albedo from the earthshine measurement from a low Earth orbit instrument. As a part of on-going technology development for SALEX instrument, we are currently developing a new Earth albedo measurement simulation tool using integrated ray tracing computation technique reported elsewhere^[14-20].

$$T_{Earth} = \left\{ \frac{S(1 - A_{Earth})}{4\sigma(1 - g)} \right\}^{\frac{1}{4}} \quad (1)$$

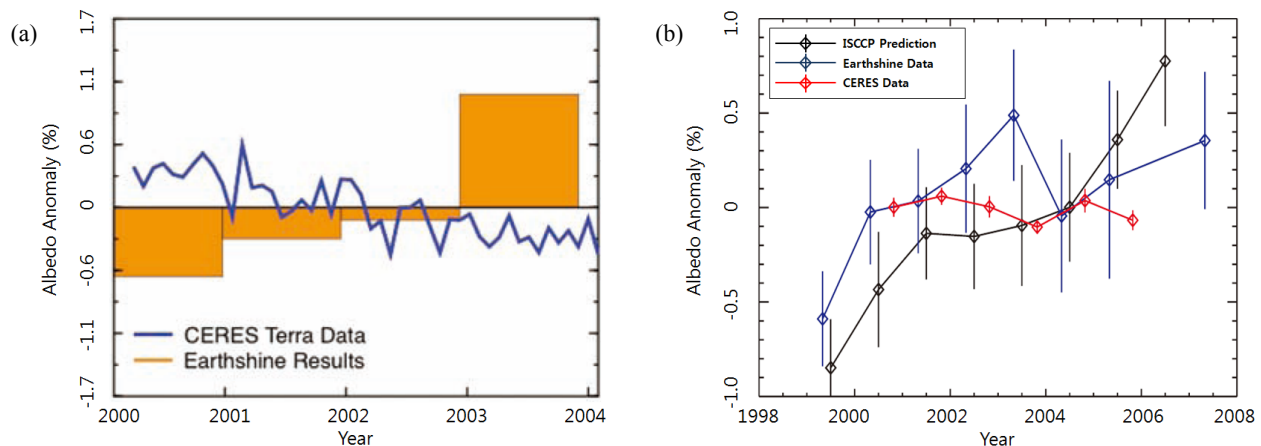


Fig. 1 Earthshine (BBSO) and CERES observation Earth albedo anomaly data; (a) Wielicki^[3], (b) Goode^[10]

As an important part of the tool development, we are currently working on a new 3D BRDF model for lunar surface. The lunar soil BRDF was first modeled by Hapke^[21-23]. The study was followed by Yuriy Shkuratov's BRDF simulation^[24]. In 1978, Hapke measured reflectance characteristics of the lunar soil sample obtained from Apollo mission and the subsequent measurements have been performed in University of Bern (PHIRE) in 2006^[25,26]. In 2009, University of California (BUG) measured the BRDF of Apollo 11 10084 sample and obtained Hapke parameters by fitting the model to the measurement data^[27,28]. However, aforementioned studies have focused the BRDF characteristics of the lunar soil, and the lunar surface reflectance and scattering characteristics in connection with earthshine measurements have never been studied in the global lunar scale up until now.

With these backgrounds, the study reports the global lunar surface BRDF model for the first time and applied it for earthshine measurement and Earth albedo estimation computation. Section 2 describes Integrated Ray Tracing (IRT) technique, approximated analytic computation for earthshine and moonshine flux measurements and the lunar BRDF model. Trial computation of the moonshine and earthshine flux is described in Section 3 and Section 4 summarizes the Earth albedo estimation before the implications in Section 5.

2. METHODS FOR EARTHSHINE AND MOONSHINE FLUX ESTIMATION

2.1 Moonshine and earthshine estimation with IRT

2.1.1 Concept of IRT computation

We are currently developing a new Monte-Carlo ray tracing computation technique reported elsewhere^[14-20]. The technique is to use "ray tracing" for simultaneous computation of imaging and radiative transfer among the light source,

measurement target and detecting instrument. For this study, it is enhanced and modified with a new lunar model (measurement target 2) added to the existing Sun (i.e. light source) and Earth (measurement target 1) models, while the detecting instrument is deleted. Fig. 2 illustrates the IRT model components and their configuration parameters used as input variables for computation.

In ray tracing, statistical Monte-Carlo computation uses 8 parameters defining a light ray. They are 3-D coordinate, direction cosine values, wavelength, radiant flux.^[30] Radiant flux is calculated with Eq. 2 when the ray encounters with optical surface. Here Φ_s is incident radiant flux, BRDF bidirectional reflectance distribution function of the target surface, θ a cross section of detection area, φ zenith and azimuth angle. The subscription s, v and e are for incident angle, scattering angle and the angle between the scattered ray and the normal direction of detection surface, n the number of the rays and R the distance between the scattering target surface and the detector.

$$\Phi_v = \Phi_s BRDF(\theta_s, \varphi_s, \theta_v, \varphi_v) \frac{a_{PA} \cos \theta_s}{nR^2} \quad (2)$$

2.1.2 Moonshine and earthshine flux estimation concept

Table 1 summarizes computational variables involved in Eq. 2 for moonshine and earthshine estimation. The “moonshine” is defined as the receiving flux at the Earth from the illuminated side of the Moon surface. In the model shown in Fig. 2, the Sun and the Moon are located in Y-Z plane and revolve around the Earth at D_{SE} ($1.496 \times 10^{11} m$) and D_{EM} ($3.800 \times 10^8 m$) in distance respectively. The Sun surface is defined as a Lambertian sphere surrounding an emitting source generating Φ_{Sun} ($1.626 \times 10^{26} W$). The light rays generated from the source are divided into 3 child rays when passing the Lambertian sphere. R_{Moon} ($1.738 \times 10^6 m$) is the radius of the Moon and D_{SM} is the distance between the Sun and the Moon that changes as the Moon revolves around the Earth. The 150,000 light rays representing the moonshine ($\Phi_{moonshine}$) is sent to the hypothetical detector at the Earth center. The Moon surface is defined with three BRDF models explained in sub-section 2.3.

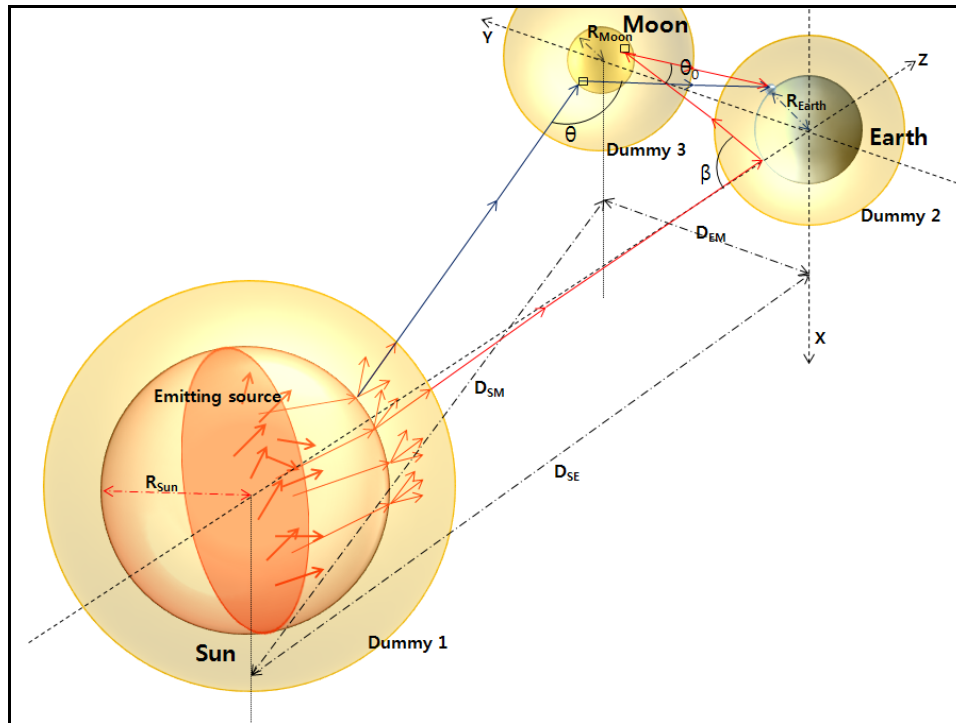


Fig. 2 Integrated Ray Tracing (IRT) geocentric coordinate

The “earthshine” is sunlight reflected from the Earth and in turn, back to the Earth from the dark side of the Moon surface^[1]. Definition of rays in Earthshine IRT case is similar to the moonshine case. With the Sun generating Φ_{Sun} ($1.626 \times 10^{26} W$) toward Earth surface, the light rays with radiant flux (Φ_{Earth_in}) travel to the Earth surface where they are reflected and scattered with 0.3 in bond albedo, following the assumption that the Earth can be regarded as a Lambertian sphere when the scattering angle is smaller than $2/3\pi$ ^[4]. The earthshine power Φ_{Earth_out} (W) arriving at the Moon surface with surface BRDF characteristics and scattered to the detector with radiant power $\Phi_{earthshine}$ (W) expressed in Table 1.

Table 1 IRT computation variables for moonshine and earthshine estimation

Type	Optical layer	Previous surface	Next surface	Φ_v	Φ_s	BRDF model	θ_s	a	R	n
Moonshine	Surface of the Sun	Inside the Sun	Moon	Φ_{Moon}	Φ_{Sun}	L	Limited by solid angle of the Moon	πR_{Moon}^2	D_{SM}	150000
	Surface of the Moon	Moon	detector	$\Phi_{moonshine}$	Φ_{Moon}	L, S, D	Limited by solid angle of the detector	$\pi R_{detector}^2$	D_{EM}	150000
Earthshine	Surface of the Sun	Inside the Sun	Earth	Φ_{Earth_in}	Φ_{Sun}	L	Limited by solid angle of the Earth	πR_{Earth}^2	D_{SE}	150000
	Surface of the Earth	Earth	Moon	Φ_{Earth_out}	Φ_{Earth_in}	L	Limited by solid angle of the Moon	πR_{Moon}^2	D_{EM}	150000
	Surface of the Moon	Moon	detector	$\Phi_{Earthshine}$	Φ_{Earth_out}	L, S, D	Limited by solid angle of the detector	$\pi R_{detector}^2$	D_{EM}	150000

Note: L (Lambertian), S (Hapke BRDF with SHG), D (Hapke BRDF with DHG)

2.2 Moonshine and earthshine estimation with finite element based analytic computation

In order to prove the validity of IRT computation of moonshine and earthshine fluxes, we developed approximated analytic equations that would produce similar results to those of IRT. The method employs the Moon surface divided into a number of finite surface elements. First, it starts with Eq. 3 that describes the position vectors of the Sun (\vec{P}_{Sun}), the Earth (\vec{P}_{Earth}) and the Moon (\vec{P}_{Moon}) shown in Fig. 2.

$$\begin{aligned}\vec{P}_{Sun} &= [0 \quad 0 \quad -D_{SE}] \\ \vec{P}_{Earth} &= [0 \quad 0 \quad 0]\end{aligned}\quad (3)$$

$$\begin{aligned}\vec{P}_{Moon} &= [0 \quad D_{EM} \sin \theta \quad D_{EM} \cos \theta] \quad (0^\circ \leq \theta \leq 180^\circ) \\ \vec{P}_{Patch} &= \begin{bmatrix} -R_{Moon} \sin \phi_i \\ M_y - R_{Moon} \cos \phi_i \sin(\theta + \delta_j) \\ M_z - R_{Moon} \cos \phi_i \cos(\theta + \delta_j) \end{bmatrix} \quad (-85^\circ \leq \phi_i \leq 85^\circ, -85^\circ \leq \delta_j \leq 85^\circ)\end{aligned}\quad (4)$$

Each lunar finite surface element has incident zenith angle (θ_{s_ij}), scattering zenith angle (θ_{v_ij}), incident azimuth angle (ϕ_{s_ij}) and scattering azimuth angle (ϕ_{v_ij}) expressed in Eq. 10. The direction vectors from a surface element to the Sun and the Earth can be written as Eq. 4 that is used to compute the Sun and Earth elevation angles from the specific surface element. Normal vector to finite surface (V_N) is a basis vector of dot and cross product to obtain surface elements of the direction vectors.

$$\begin{aligned}
\bar{V}_{PS} &= \bar{P}_{Sun} - \bar{P}_{Patch} \\
\bar{V}_{PE} &= \bar{P}_{Earth} - \bar{P}_{Patch} \\
\bar{V}_N &= \bar{P}_{Patch} - \bar{P}_{Moon}
\end{aligned} \tag{5}$$

For the moonshine estimation, the arriving radiant flux at a lunar surface element can be computed from Eq. 6, where $a_{i,j}$ is projected area. For the earthshine case, the radiant flux (Φ_{Sun}) of the Sun is converted to irradiance (E_{Earth_in}) via Eq. 7, when the light rays arrive at the Earth. Then the earthshine intensity I_{Earth} (W/m^2) can also be defined as Eq. 8^[29] after being scattered from the Lambertian surface of the Earth, where A_{Earth} is the Earth albedo, R_{Earth} the Earth radius R_{Earth} ($6.378 \times 10^6 m$) and β ($^\circ$) the Earth phase as viewed from the Moon. This leads to the arriving radiant flux ($E_{Earth_out_i,j}$) at a lunar surface element as expressed in Eq. 9.

$$\Phi_{Moon_i,j} = a_{i,j} \frac{\Phi_{Sun}}{4\pi D_{SM}^2} \tag{6}$$

$$E_{Earth_in} = \frac{\Phi_{Sun}}{4\pi D_{SE}^2} \tag{7}$$

$$I_{Earth} = \frac{A_{Earth} R_{Earth}^2 E_{Earth_in}}{\pi} [(\pi - \beta) \cos(\beta) + \sin(\beta)] \tag{8}$$

$$\Phi_{Earth_out_i,j} = I_{Earth} \Omega_{EM_i,j} \tag{9}$$

Using the above mentioned equations, the arriving intensity $I_{i,j}$ from a lunar surface element back to the Earth center can be computed from Eq. 10. ($\Phi_{x_i,j}$) arriving radiant flux at the lunar surface element for moonshine or earthshine case, $\theta_{s_i,j}$ incident zenith angle, $\theta_{v_i,j}$ scattering zenith angle and $\phi_{s_i,j}$ incident azimuth angle and $\phi_{v_i,j}$ scattering azimuth angle. The arriving moonshine or earthshine flux (Φ_x) at the detector can then be estimated using Eq. 11, where Ω_O is detector solid angle.

$$I_{i,j} = \Phi_{x_i,j} BRDF(\theta_{s_i,j}, \phi_{s_i,j}, \theta_{v_i,j}, \phi_{v_i,j}) \tag{10}$$

$$\Phi_x = \sum_{\theta=0^\circ}^{180^\circ} \sum_{\phi_i=-85^\circ}^{85^\circ} \sum_{\phi_j=-85^\circ}^{85^\circ} I_{i,j} \cos(elevation) \Omega_O \tag{11}$$

2.3 3D lunar BRDF models

In IRT computation of earthshine and moonshine fluxes, the lunar surface is represented as a 3D spherical surface of Hapke BRDF model^[21-23]. For smooth and semi-infinite surface, Hapke BRDF model can be expressed as in Eq. 12 where w is single scattering albedo, $B(g)$ back scattering function, $P(g)$ Henyey-Greenstein phase function, $H(x)$ multiple scattering function, g scattering angle and μ & μ_0 are $\cos(\theta_{s_i,j})$ and $\cos(\theta_{v_i,j})$. In particular, two types of Henyey-Greenstein phase function are used in this study. The first one is Single Henyey-Greenstein phase function (SHG) show single scattering lobe across all the scattering angle and it is expressed as in Eq. 13 where ξ is the cosine asymmetric factor, $\xi = \langle \cos\theta \rangle = -\langle \cos(g) \rangle$. The second is Double Henyey-Greenstein phase function (DHG) having double scattering lobes for forward and back scattering angles and it is defined as Eq. 14, where b and c are scattering lobe's width and height.

$$HapkeBRDF(\theta_{s_{i,j}}, \theta_{v_{i,j}}, g_{i,j}) = \frac{w}{4\pi} \frac{1}{\mu_0 + \mu} \{ [1 + B(g)]p(g) + H(\mu_0)H(\mu) - 1 \} \quad (12)$$

$$P_{SHG}(g) = \frac{1 - \xi^2}{(1 + 2\xi \cos g + \xi^2)^{3/2}} \quad (13)$$

$$P(g)_{DHG} = \frac{1+c}{2} \frac{1-b^2}{(1+2b \cos g + b^2)^{3/2}} + \frac{1-c}{2} \frac{1-b^2}{(1-2b \cos g + b^2)^{3/2}} \quad (14)$$

Using input Hapke parameters listed in Table 2^[27,28], Hapke BRDF model for SHG and DHG were used to compute reflectance factor against scattering zenith angle ($\theta_{v_{i,j}}$) for 75° incident zenith angle ($\theta_{s_{i,j}}$) of incident light. The result are shown in Fig. 4a (azimuth angle = 0°) and Fig. 4b (azimuth angle = 90°). Red solid lines are from SHG and blue dashed lines are from DHG. From Fig. 3, we note that i) the Hapke BRDF with SHG agree well with the measurement for the scattering zenith angle range of -20° ~ +80° (i.e. toward the forward scattering), whereas it tends to depart from the measurement for the scattering angle of -20° ~ -90° (i.e. toward the back scattering) and ii) the Hapke BRDF with DHG shows relatively good agreement with the measurement, although it has slightly different curve from that of the existing study^[27,28].

Table 2 Hapke parameters for smooth and semi-infinite case^[27,28]

Parameter	λ	w	h	$B0$	ζ	b	c
Hapke(SHG)	750 nm	0.33	0.017	1	- 0.075	-	-
Hapke(DHG)	750 nm	0.33	0.017	1	-	0.308	0.425

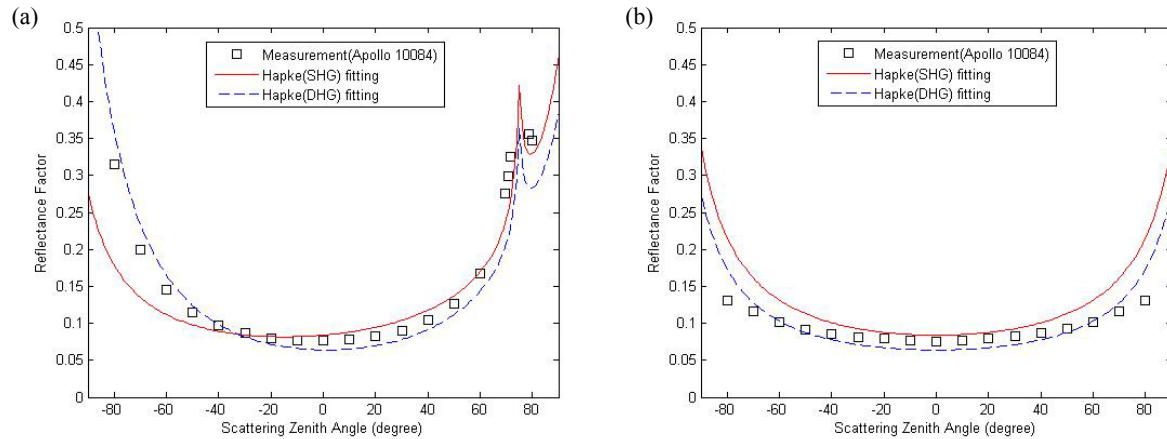


Fig. 3 Computed and measured reflectance factors, (a) azimuth angle 0° and (b) azimuth angle 90°

3. IRT SIMULATION RESULTS

3.1 Ray tracing test with Hapke BRDF models

Since IRT tool has been developed in ASAPTM environment, we checked the accuracy and validity of the ray tracing computation with Hapke BRDF integrated into ASAP. In this ray tracing simulation, the source is defined as a grid source of $0.5m$ in radius and set to 75° in incident zenith angle. The target is a circular plane of $2.5m$ in radius and located at $10m$ distance. The detector plane of $0.5m$ in radius is positioned at $200m$ in distance. The plane is rotated by 5° in each zenith angle step while its azimuth angle remains stationary. We then calculated arriving flux at the detector plane. It was subsequently used to compute the BRDF data in ASAP format by having the ratio between irradiance and radiance. Fig. 4 shows the resulting BRDF for 75° in incident zenith angle and 0° in azimuth angle. The open square symbols are the ray tracing simulation results, whereas the solid lines are computed using analytic Eq. 12. The results show a good agreement (i.e. 2.28% for SHG and 0.01% for DHG) between the simulation and analytic computation, proving that the Hapke BRDF model can be integrated into ASAP based IRT ray tracing while ensuring the computation accuracy.

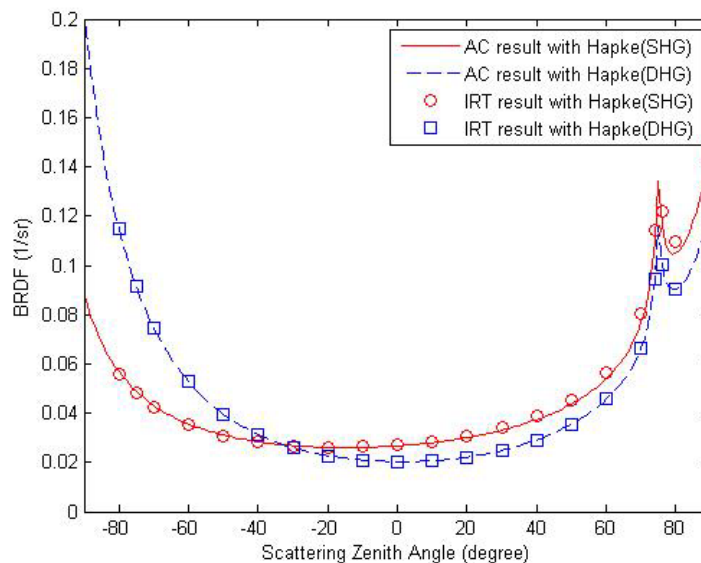


Fig. 4 Small scale BRDF test

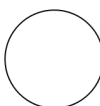
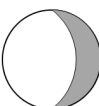
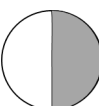
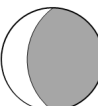
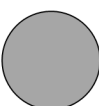
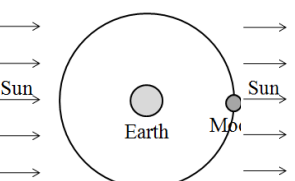
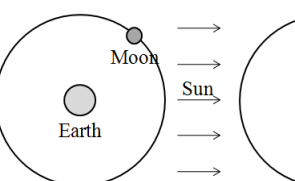
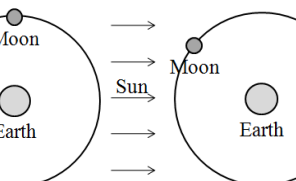
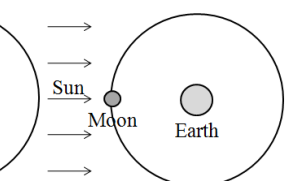
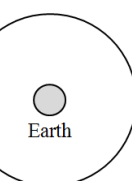
3.2 Moonshine and earthshine estimation with lunar BRDF models

As listed in Table 3, three BRDF models were used to represent 3 different lunar surfaces: i) Lambertian (L) ii) Hapke BRDF with SHG and iii) Hapke BRDF with DHG. The Sun and the Earth were fixed in the coordinate system while the Moon revolves around the Earth from 0° to 180° in 5° angular step in phase (see Table 4). For IRT computation, 50000 rays were generated from the source and traced, and the simulation was run 10 times for each phase angle. The standard deviation of ray tracing simulation results is about 0.2%. The resulting moonshine and earthshine fluxes are shown in Fig 5a and Fig. 5b respectively. The cross symbols are the results from IRT simulation and the solid lines are from the aforementioned analytic computation described in Section 2. We note that the difference between the IRT simulation and analytic computation is about 2% for moonshine flux and 6.8% for earthshine flux, proving validity of the IRT simulation with Hapke BRDFs. Specially, the earthshine fluxes from the Hapke BRDFs with SHG and DHG are almost identical. This is caused by smaller than 1° in the difference between incident and scattering zenith angles and, for such small angular difference, the scattering lobes from the two phase functions show virtually no difference. Hence, the earthshine flux curves look almost identical to each others.

Table 3 Ray path and optical models used in moonshine and earthshine simulation

Table 3 Ray path and optical models used in moonshine and earthshine simulation								
Moonshine	Ray path	Sun	→	Moon	→	Detector	-	
	Optical model	Lambertian		<i>L, SHG, DHG</i>		Absorption	-	
Earthshine	Ray path	Sun	→	Earth	→	Moon	→	Detector
	Optical model	Lambertian		Lambertian		<i>L, SHG, DHG</i>		Absorption

Table 4 Simulation case definition for Moon phases

Moon Phase	0°	45°	90°	135°	180°
Shape of the Moon					
Position of the Moon					

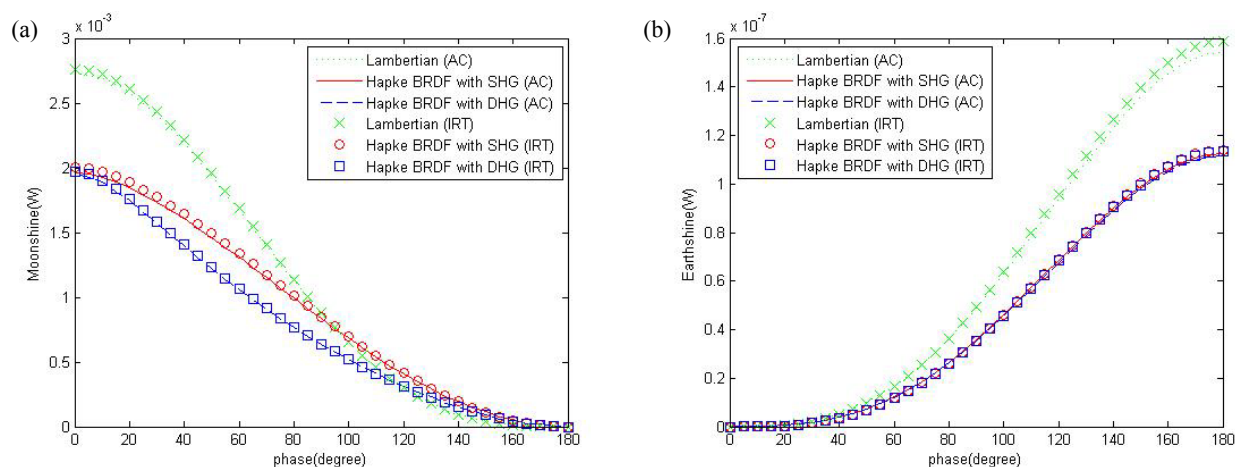


Fig. 5 (a) Moonshine and (b) Earthshine calculation data

4. EARTH ALBEDO ESTIMATION

4.1 Geometrical Earth albedo and apparent Earth albedo calculation

The Earth geometric albedo p_E can be computed from Eq. 15^[1] where $f_E(\beta)$ is the Earth's phase function, p_a and p_b are lunar albedo caused by scattering of earthshine and moonshine ($p_a = p_b$ in this computation), f_a and f_b are Moon phase functions, and E_a and E_b earthshine and moonshine irradiances. The Earth apparent albedo (p^*) can also be computed by using Eq. 16^[1]. Fig. 6 shows the resulting albedo plotted against phase angle. Fig. 6a shows all three BRDF models producing very similar geometric albedo data both in analytic and ray tracing computations. In the mean time, Fig. 6b is apparent albedo data exhibiting the difference between ray tracing and analytic computation over 0°-90° in phase angle. It is caused by decreasing number of rays used for the earthshine computation as the moon phase approaches to the full moon.

$$p_E f_E(\beta) = \frac{p_b f_b(\theta)}{p_a f_a(\theta_0)} \frac{E_a}{E_b} \frac{D_{EM}^2 D_{SE}^2}{R_E^2 D_{SM}^2} \quad (15)$$

$$p^*(\beta) = \frac{3}{2 f_L(\beta)} \frac{p_b f_b(\theta)}{p_a f_a(\theta_0)} \frac{E_a}{E_b} \frac{D_{EM}^2 D_{SE}^2}{R_{Earth}^2 D_{SM}^2} \quad (16)$$

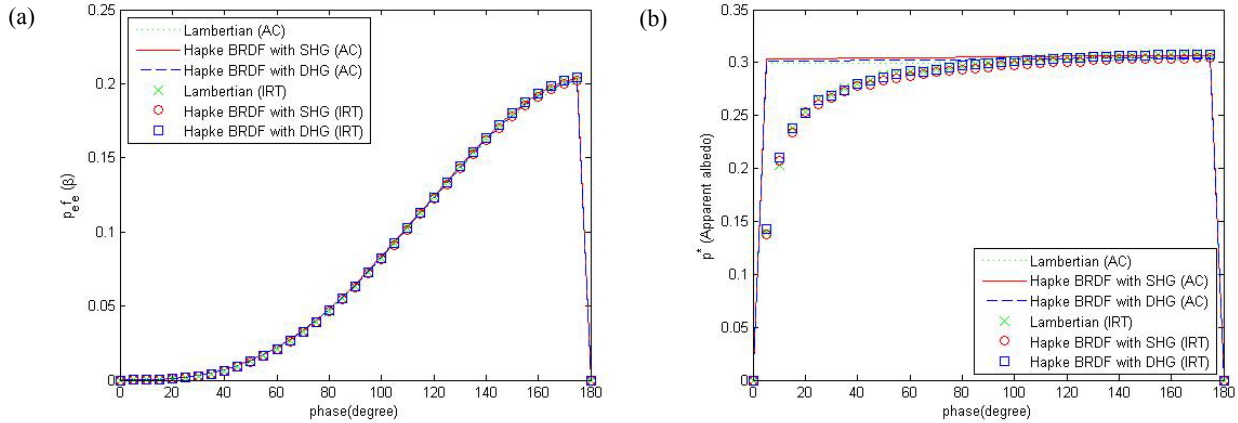


Fig. 6 (a) Geometric albedo and (b) apparent albedo calculation data

4.2 Earth bond albedo

The Earth bond albedo can be computed using the apparent albedo as in Eq. 17 below^[1] where A is Earth bond albedo, β is Earth phase angle and $f_L(\beta)$ is Earth phase function. For the input Earth albedo of 0.3 in Lambertian scattering, the analytic computation and ray tracing simulation produced the output albedo data listed in Table 5 for three different lunar surface BRDF models described in earlier sections. The differences between the input and output albedo values are small and it proves that the analytic calculation and IRT simulation can be used to estimate the earth bond albedo within about 1% in accuracy, even when the input albedo varies.

$$A = \frac{2}{3} \int_{-\pi}^{\pi} d\beta p^*(\beta) f_L(\beta) \sin \beta \quad (17)$$

Table 5 Output Earth Bond Albedo derived from apparent albedo for input bond albedo of 0.3

Output Earth bond albedo	Computation method	Lambertian(0.10)	SHG	DHG
A	Analytic Calculation	0.3009	0.3057	0.3035
	IRT Calculation	0.3030	0.2993	0.3026

5. CONCLUDING REMARKS

In this study, we introduce the BRDF based global lunar surface model to the relevant academic community for the first time. The lunar surface BRDF models were used in ray tracing and analytic computation of radiative transfer among the Sun, the Earth and the Moon. The computed variables include moonshine and earthshine fluxes followed by estimation of the Earth apparent and bond albedo outputs. The resulting Earth bond albedo (both analytically computed and ray tracing simulated) agree well with the input Earth albedo of 0.3 within about 1% in difference. Whilst we acknowledge that the current IRT model components need further improvements, the trial investigation reported in this study brings technical confidence to the conceptual validity and applicability of the IRT model for space earthshine measurement for accurate estimation of the Earth bond albedo variation that influences current and future global warming rates.

REFERENCES

- [1] Qiu, J., Goode, P. R., Palle, E., Yurchyshyn, V., Hickey, J., Montanes Rodriguez, P., Chu M.-C., Kolbe, E., Brown, C. T., and Koonin, S. E., "Earthshine and the Earth's albedo: 1. Earthshine observations and measurements of the lunar phase function for accurate measurements of the Earth's Bond albedo," *Journal of Geophysical Research*, 108(D22), 4709, 12-1–12-22 (2003).
- [2] Wielicki, B. A., Barkstrom, B. R., Harrison, E. F., Ill, R. B. L., Smith, G. L., and Cooper, J. E., "Clouds and the Earth's Radiant Energy System (CERES): An Earth Observing System Experiment," *Bulletin of the American Meteorological Society* 77, 5, 853-868 (1996).
- [3] Wielicki, B. A., Wong, T., Loeb, N., Minnis, P., Priestley, K., and Kandel, R., "Changes in Earth's Albedo Measured by Satellite," *Science* 308, 825 (2005).
- [4] Goode, P. R., Qiu, J., Yurchyshyn, V., Hickey, J., "Earthshine observations of the Earth's reflectance," *Geophysical Research Letters* 28, No. 9, 1671-1674 (2001).
- [5] Palle, E., Goode, P. R., and Montanes-Rodriguez, P., and Koonin, S. E., "Changes in Earth's Reflectance over the Past Two Decades," *Science* 304, 1299–1301 (2004).
- [6] Palle, E., Montanes-Rodriguez, P., Goode, P. R., Qiu, J., Yurchyshyn, V., Hickey, J., Chu, M.-C., Kolbe, E., Brown, C. T., and Koonin, S. E., "The Earthshine Project : update on photometric and spectroscopic measurements," *Advances in Space Research* 34, 288-292 (2004).
- [7] Palle, E., Goode, P. R., Montanes-Rodriguez, P., Koonin, S. E., and Rumyantsev, V., "Toward a global earthshine network: First results from two stations," *Geophysical Research Letters* 32, L11803, 1-4 (2005).
- [8] Montanes-Rodriguez, P., Palle, E., Goode, P. R., Hickey, J., and Koonin, S. E., "Globally Integrated Measurements of the Earth's Visible Spectral Albedo," *Astrophysics Journal*, 629, 1175-1182 (2005).
- [9] Montanes-Rodriguez, P., Palle, E., Goode, P. R., and Martin-Torres, F. J., "Vegetation Signature in the Observed Globally Integrated Spectrum of Earth Considering Simultaneous Cloud Data: Applications for Extrasolar Planets," *ApJ* 651, 544-552 (2006).
- [10] Palle, E., Goode, P. R., and Montanes-Rodriguez, P., "Interannual variations in Earth's reflectance 1999-2007," *Journal of Geophysical Research*, Vol. 114, D00D03 (2009).
- [11] WCRP/IAMAP/RC, "A Preliminary Cloudless Standard Atmosphere for Radiation Computation," WCP 112 WMO TDNo. 24, 1-xx (1986).
- [12] Lockwood, M., "Long-term variations in the open solar flux and possible links to Earth's climate; From Solar Min to Max: Half a solar cycle with SoHO", *Proc. SoHO 11 Symposium*, Davos, ESA-SP-508, pp 507- 522, ESA Publications (2002).
- [13] Lee, J.-M., Technical Report SALEX-TR001-JL (2007).
- [14] Lee, J.-M., "Integrated ray tracing model for end-to-end performance verification of Amon-Ra instrument," Master's thesis, Graduate School of Yonsei University (2006).
- [15] Ham, S.-J., "Red tide detection simulation for integrated ray tracing model in-orbit Performance verification with GOCL," Master's thesis, Graduate School of Yonsei University (2007).
- [16] Sung S.-H., "Efficient ray-tracing computational technique for in-orbit performance prediction for improved Amon-Ra energy channel instrument," Master's thesis, Graduate School of Yonsei University (2010).

- [17] Yoon, J.-Y., "Optimized baffle and vane design for stray light suppression for Amon-Ra visible channel instrument," Master's thesis, Graduate School of Yonsei University (2007).
- [18] Sung S.-H., Yu, J.-H., Ryu, D.-O., Hong, J.-S., Yoon J.-Y., Kim, S.-W., Lee, J.-H., and Shin, M.-J., "Imaging and radiometric performance simulation for a new high-performance dual-band airborne reconnaissance camera," Proc. SPIE 7307, 730705-1-13 (2009).
- [19] Ryu, D.-O., Sung S.-H., Lee, J.-M., Hong, J.-S., Jeong, S.-M., Jeong, Y.-K., and Kim, S.-W., "Integrated Ray Tracing Simulation of Spectral Bio-signatures from Full 3-D Earth Model," Proc. SPIE 7441, 74410A-1-11 (2009).
- [20] Ryu, D. O., Kim, S.-W., Kim, D.-W., Lee, J.-M., Lee, H.-S., Park, W.-H., Sung S.-H., and Ham, S.-J., "Integrated ray tracing simulation of annual variation of spectral bio-signature from cloud free 3D optical Earth model," Proc. SPIE 7819, 78190E-1-14 (2010).
- [21] Hapke, W. B., "Bidirectional Reflectance Spectroscopy; 1. Theory", Journal of Geophysical Research, Vol. 86, No. B4, 3039-3054 (1981).
- [22] Hapke, W. B., [Theory of reflectance and Emittance spectroscopy], Cambridge University Press (1993).
- [23] Hapke, W. B., "Bidirectional Reflectance Spectroscopy; 5. The Coherent Backscatter Opposition Effect and Anisotropic Scattering," Icarus 157, 523-534 (2002).
- [24] Shkuratov, Y., and Starukhina, L., "A Model of Spectral Albedo of Particulate Surfaces; Implications for Optical Properties of the Moon," Icarus 137, 235-246 (1999).
- [25] Hapke, W. B., Partlow, W. D., Wagner, J. K., and Cohen, A. J., "Reflectance measurements of lunar materials in the vacuum ultraviolet," 9th Lunar and Planetary Science Conference, 2935-2947 (1978).
- [26] Gunderson, K., Thomas, N., Whitby, J. A., "First measurements with the Physikalisches Institut Radiometric Experiment (PHIRE)," Planetary and Space Science, 54, 1046-1056 (2006).
- [27] Foote, E. J., Paige, D. A., Johnson, J. R., Grundy, W. M., and Shepard, M. T., "The Bidirectional Reflectance of Apollo 11 Soil Sample 10084," 40th Lunar and Planetary Science Conference, 2500 (2009).
- [28] Johnson, J. R., Shepard, M. K., Paige, D. A., Foote, E. J., and Grundy, W., "Spectrogoniometric Measurements And Modeling Of Apollo 11 Soil 10084," 40th Lunar and Planetary Science Conference, 1427 (2009).
- [29] Look, Jr., D. C., "General Expression for Lambert Diffuse Reflection," Book review 'Progress in Optics, Vol.3' (1964).
- [30] Breault Research Organization, "User Guide; ASAP Reference Guide", <http://www.breault.com/k-base.php> (2011).

ACKNOWLEDGEMENT

This research was supported by Basic Science Research Program through the National Research Foundation of Korea (NRF) funded by the Ministry of Education, Science and Technology (2011-0003958). We acknowledge the support of Breault Research Organization through the user licenses for Advanced System analysis Program (ASAPTM) for ray tracing computation.